Study of vertical upward flame spread on charring materials-Part II: Numerical simulations

Wasan, S.R., Rauwoens, P., Vierendeels, J. and Merci, B.

In: Fire and Materials 35 (5), 261-273, 2011.

Study of Vertical Upward Flame Spread on Charring Materials – Part II: Numerical Simulations

S.R. Wasan, P. Rauwoens, J. Vierendeels and B. Merci

Ghent University – UGent, Department of Flow, Heat and Combustion Mechanics

Corresponding author: Bart.Merci@UGent.be

Abstract

Simulation results, obtained by means of application of an enthalpy based pyrolysis model, are presented. The ultimate focus concerns the potential of the model to be used in flame spread simulations. As an example we discuss vertically upward flame spread over a charring material in a parallel plate configuration. Firstly, the quality of the pyrolysis model is illustrated by means of cone calorimeter results for square (9.8 cm x 9.8 cm exposed area), 1.65cm thick, horizontally mounted MDF samples. Temperatures are compared at the front surface and inside the material, for different externally imposed heat fluxes (20 kW/m^2, 30 kW/m^2 and 50 kW/m^2), for dry and wet samples. The mass loss rate is also considered. Afterwards, vertically upward flame spread results are reported for large particle board plates (0.025 m thick, 0.4 m wide and 2.5 m high), vertically mounted face-to-face, for different horizontal spacing between the two plates. The simulation results are compared to experimental data, indicating that, provided that a correct flame height and corresponding heat flux are applied as boundary conditions, flame spread can be predicted accordingly, using the present pyrolysis model.

1. Introduction

In part I [1], the outcome of an experimental campaign was reported. In the present paper, we apply a simple pyrolysis and evaporation model, based on enthalpy [2], to the same configurations.

Firstly, we discuss the one-dimensional cone calorimeter configurations.

Afterwards, vertically upward flame spread in a parallel plate configuration is considered. By no means, it is our intention to introduce a (semi-empirical) flame spread model, to be used for other configurations than the specific one considered here. The only objective is to illustrate that the developed pyrolysis model is ready-to-use for such configurations and that reasonably accurate results can be obtained, provided an appropriate value for incoming heat flux onto the solid material is provided. This heat flux could stem from CFD (Computational Fluid Dynamics) in the gas phase, where the turbulent combustion is simulated. However, we do not use CFD in the present paper, as uncertainties in CFD would distract the attention from our objective as mentioned. Rather, we use experimental data [1] to estimate the heat fluxes that serve as boundary conditions for the simulations. In this sense, the set-up is somehow a sophism, but this suffices for the sake of the present paper, as explained above. The major advantage is that the strong sensitivity of flame heat fluxes to e.g. fuel sootiness [3, 4] is avoided. To summarise, expressions as developed in [3] for a similar set-up as the one under study in the present paper, are not applied here, but the present paper is not intended to provide an alternative for such relationships.

2. Numerical simulations set-up

2.1 Model description

In [2, 5], the model, along with the solution procedure, is extensively described and applied to some basic configurations. The reader is referred to those references for all details. We only recall here that the model relies on a fixed computational mesh, which can be relatively coarse. On this mesh, the energy equation is solved numerically. Pyrolysis (and evaporation) is modelled as an infinitely fast irreversible process, taking place at an infinitely thin front at 'pyrolysis' (resp. 'evaporation') temperature. Thus, fronts are moving through the solid material. As the evaporation front passes, wet virgin material becomes dry virgin material. As the pyrolysis front passes, dry material becomes char. In the present simulations, the water vapour and pyrolysis gases are assumed to leave the solid instantaneously. They are in thermal equilibrium with the solid. More advanced pyrolysis modelling (e.g. [6]) is possible, but this is beyond the scope of the present paper.

2.2 Cone calorimeter set-up

We first discuss the results for the cone calorimeter set-up of [1]. We consider one-dimensional heat transfer in the solid [1]. The computational mesh in the solid, with thickness 1.65 cm, contains 33 cells. The time step size is set to 0.5s. It has been verified that the results presented do not vary when more cells or smaller time steps are chosen.

The externally imposed heat flux $\dot{q}''_{ext}$ equals 20 kW/m^2, 30 kW/m^2 or 50 kW/m^2. The experiments were performed in open atmosphere, so that flames appear when the volatiles are ignited with a spark ignition placed above the retainer frame. These flames provide additional heat flux to the solid during pyrolysis. In the simulations, this is

modelled as an additional heat flux at the front surface. We assume the heat flux from the flames, absorbed by the material, constant throughout the experiment, equal to $\dot{q}''_{flame,abs} = 10 kW/m^2$. The rationale is that, even though the flame height varies during the experiments [1], the radiative flux need not change too much as long as the maximum temperature does not change significantly. The value of 10 kW/m^2 is a rough estimate. For flames of 700 ^{o}C (see below), this corresponds to a net absorption by the front surface of 20% of the black body emissive power of the flames. Note that the same value was reported for the experiments in [7] on pine samples. The radiation loss from the front surface to the surroundings is also explicitly considered.

For the convective boundary condition at the front surface, the ambient temperature is set to the initial room temperature (T_{amb} = 300 K) until pyrolysis takes place. From then on, until the end of pyrolysis, the surface is assumed to see flames, rather than air at approximately ambient temperature. We model this effect by setting the heat exchange temperature for convection at the surface equal to T_{flame} = 700 ^{o}C, an estimate for the flame temperatures, based on the plateaus observed in the surface temperatures during pyrolysis (Fig. 2 below). As soon as the pyrolysis ends, i.e. as soon as the pyrolysis front reaches the back surface, the flame heat flux decays exponentially from 10 kW/m^2, with a decay time constant equal to τ_{flame} = 30 s. Three minutes later, as in the experiments [1], the externally imposed heat flux is switched off as well. The time constant for this exponential decay is set to τ = 600 s, due to the thermal inertia of the heated coil in the cone. The time constants have been chosen so as to resemble the experimentally observed temperature decays with a sufficient level of accuracy (see below).

The back surface is perfectly insulated and impervious to volatiles.

The boundary conditions at the exposed front surface are summarised as follows:

- prior to pyrolysis ($0 < t < t_{start}$):

$$\dot{q}''_{net} = \varepsilon \dot{q}''_{ext} - h\left(T_s - T_{amb}\right) - \varepsilon\sigma\left(T_s^4 - T_{amb}^4\right) \quad (1a)$$

- during pyrolysis ($t_{start} < t < t_{end}$):

$$\dot{q}''_{net} = \varepsilon \dot{q}''_{ext} + \dot{q}''_{flame,abs} - h\left(T_s - T_{flame}\right) - \varepsilon\sigma\left(T_s^4 - T_{amb}^4\right) \quad (1b)$$

- immediately after pyrolysis ($t_{end} < t < t_{end} + 180s$):

$$\dot{q}''_{net} = \varepsilon \dot{q}''_{ext} + \dot{q}''_{flame,abs} \exp\left(-\frac{t - t_{end}}{\tau_{flame}}\right) - h\left(T_s - T_{flame}\right) - \varepsilon\sigma\left(T_s^4 - T_{amb}^4\right) \quad (1c)$$

- more than three minutes after the end of pyrolysis ($t > t_{end} + 180s$):

$$\dot{q}''_{net} = \varepsilon \dot{q}''_{ext} \exp\left(-\frac{t - t_{end} - 180}{\tau}\right) + \dot{q}''_{flame,abs} \exp\left(-\frac{t - t_{end}}{\tau_{flame}}\right) - h\left(T_s - T_{flame}\right) - \varepsilon\sigma\left(T_s^4 - T_{amb}^4\right)$$

(1d)

The (natural) convection coefficient is set to h = 10 W/(m^{2}K). The emissivity is set equal to ε = 0.9.

Table 1 summarizes the model parameters and the material properties.

[INSERT TABLE 1]

The densities were obtained by measuring the weight of wet and dry samples, along with their volume [1]. The other values have been taken from the literature [8]. Important model parameters are the heat of pyrolysis and the pyrolysis temperature [2]. The latter value has been adopted from [1], where it was shown that, depending on the externally imposed heat flux, pyrolysis starts when the front surface reaches a temperature in the range of 300 – 350 ^{o}C.

2.3 Vertically upward flame spread

The particle boards in the experiments [1] have dimensions 2.5 m (height) x 0.4 m (width) x 0.025 m (thickness). We simplify to a two dimensional case in numerical simulation, using 2.5 m x 0.025 m particle board with 100 x 40 cells for computation. A time step size of 0.5 s is used. It has been verified that the results presented do not vary when more cells or smaller time steps are chosen.

Tables 2 and 3 summarize the model parameters for the inter-plate distances of 10.5 cm and 30.5cm.

[INSERT TABLE 2]

[INSERT TABLE 3]

The back surface of the plate is assumed perfectly insulated and impervious.

The front surface boundary conditions are summarised as follows:

- prior to pyrolysis ($0 < t < t_{start}$):

$$\begin{aligned} y < y_{pfr} &: \dot{q}''_{net} = \dot{q}''_{pfr} - h\left(T_s - T_{amb}\right) - \varepsilon \cdot F.\sigma\left(T_s^4 - T_{amb}^4\right) \\ y > y_{pfr} &: \dot{q}''_{net} = \dot{q}''_{pfr} \cdot \exp\left(-C_{pfr}\left(y - y_{pfr}\right)\right) - h\left(T_s - T_{amb}\right) - \varepsilon \cdot F.\sigma\left(T_s^4 - T_{amb}^4\right) \end{aligned} \quad (2a)$$

- after onset of pyrolysis ($t > t_{start}$):

$$\begin{aligned} y < y_{pfr} &: \dot{q}''_{net} = \dot{q}''_{pfr} - h\left(T_s - T_{amb}\right) - \varepsilon \cdot F.\sigma\left(T_s^4 - T_{amb}^4\right) \\ y_{pfr} < y < y_f &: \dot{q}''_{net} = \dot{q}''_{f} - h\left(T_s - T_{amb}\right) - \varepsilon \cdot F.\sigma\left(T_s^4 - T_{amb}^4\right) \\ y > y_f &: \dot{q}''_{net} = \dot{q}''_{f} \cdot \exp\left(-C_{f}\left(y - y_{f}\right)\right) - h\left(T_s - T_{amb}\right) - \varepsilon \cdot F.\sigma\left(T_s^4 - T_{amb}^4\right) \end{aligned} \quad (2b)$$

The burner flames heat flux is modelled as a constant heat flux $\dot{q}''_{pfr}$ onto the particle board over a certain height: visual observations [1] show a ‘persistent flame region’ of height y_{pfr}. At higher heights an exponential decay is introduced as

$\dot{q}''_{pfr} \cdot \exp\left(-C_{pfr}\left(y - y_{pfr}\right)\right)$, in order to resemble the decrease of radiative heat flux. The decay constant C_{pfr} is tuned to match the temperature measurements [1] to a reasonable extent. Figure 1 gives an impression of the imposed heat flux, prior to pyrolysis, along with temperature measurements after 20s for the two inter-plate distances. For the inter-plate distance 10.5cm, $\dot{q}''_{pfr}$ is reduced to $15 kW/m^2$ for y < 0.3m to account for the incomplete combustion due to lack of oxygen [1]. This is also the reason why a lower value for $\dot{q}''_{pfr}$ is used than for the 30.5 cm inter-plate distance [1]. The decay constant is lower as the flame region is elongated. The decay constants were finally chosen such that the temperature evolutions in time at different heights (figures 7 and 8) resemble the experimental observations to a sufficient level of accuracy.

As soon as T_s=T_{pyr} at a certain height, pyrolysis starts, with the release of volatiles. These volatiles burn with oxygen to form flames. The flame heat flux is considered constant in the numerical simulations, equal to $\dot{q}''_f = 55 kW/m^2$, in the region $y_{pfr} < y < y_f$, with y_f the vertical position of the flame tip. This corresponds to a flame temperature equal to about 720^{o}C (black body radiation) if all heat is absorbed. In contrast to the cone calorimeter set-up, now indeed practically all radiation from the flames falls onto the plates. An exponential decay is assumed for $y > y_f$ again, with the same decay constant as for the persistent flame region flames ($C_f = C_{pfr}$). The flame height evolution in time is prescribed as a parabolic fit or as a piecewise linear approximation of the visually observed flame heights in time (fig. 12 of [1], repeated as figure 5 below). For the sand burner, the parabolic fit reads $y_f = 1.422 \cdot 10^{-5} t^2$, while for the honeycomb burner it reads $y_f = 1.323 \cdot 10^{-4} t^2$. We come back to this in the results section.

The ambient temperature is set to T_{amb} = 300 K. The natural convection between the plates is enhanced by an imposed flow due to exhaust gas extraction. Therefore, we set the convection coefficient to h = 15 W/(m^{2}K) here, in line with the value reported in [3]. Radiation loss from the surface to the environment of one plate is reduced by the presence of the parallel plate. As the set-up is in principle symmetric, the net radiative heat exchange between the plates is relatively small, but the heat loss from each surface to the surroundings is certainly reduced. This can be determined from the view factor for two parallel plates [9]. With the dimensions of the plates, the view factor is about 0.4 for the inter-plate distance of 30.5 cm and about 0.7 for the distance of 10.5 cm. The view factor to the environment, determining the radiative losses, equals 1 minus these values. Therefore, we introduce a correction factor to the emissivity $\varepsilon=0.9$ in the heat loss term equal to $F = 2/3$ for the distance 30.5 cm and $F = 1/3$ for the distance 10.5 cm.

3. Discussion of the results

3.1 Cone calorimeter results

3.1.1 Dry samples

Three different levels of externally imposed heat flux are applied on the MDF boards: $\dot{q}''_{ext}$ = 20 kW/m^2, 30 kW/m^2 and 50 kW/m^2. Figure 1 shows the temporal evolutions of the temperature, at the front surface (left) and at depth equal to 5 mm (right) for the dry samples. The smooth dark line is the simulation result.

The surface temperature immediately rises due to the external radiation flux (expression (1a)). Agreement between simulation results and experimentally measured values is very good. As the surface temperature reaches the pyrolysis temperature (T_{pyr} = 325 ^{o}C = 598K), the temperature starts to rise more rapidly due to the additional heat flux from the flames (1b). The time at which this happens, depends on the value of $\dot{q}''_{ext}$: the higher this value, the sooner the flames appear. This is well captured in the model. At the beginning of the pyrolysis stage, the simulation results deviate somewhat from the experiments, in particular for the lower values of $\dot{q}''_{ext}$. Obviously, the lower the value for $\dot{q}''_{ext}$, the more sensitive the results become to the flame heat flux. As time proceeds, the surface temperature in the simulations clearly evolves towards the experimental 'steady state' front surface temperature value.

After a while, the pyrolysis process ends. In the simulations, this happens at the moment the pyrolysis front reaches the back surface of the sample (see also below in the discussion of figure 3). The flames then disappear, which is modelled in the simulations by boundary condition (1c). This immediately results in a drop in the surface

temperature, in quite good agreement with the experiments (see e.g. at about 950 s in the figure for $\dot{q}''_{ext}$ =30 kW/m^2). Three minutes later, the external heat flux is switched off in the experiments [1], modelled in the simulations as described in (1d). This leads to a final front surface temperature decay.

For obvious reasons, the boundary conditions also affect the evolutions inside the material. We discuss results at depth d = 5 mm (figure 1, right). The initial temperature rise in the simulations, during the heat-up phase, is too rapid. Presumably, this is due to the neglect of remaining moisture in the sample in the simulations, since the agreement for wet samples in the heat-up phase is better (see below, discussion of figure 2). The agreement clearly improves once the pyrolysis process started. The agreement remains good as long as the pyrolysis phase continues, although over-predictions are observed for the highest $\dot{q}''_{ext}$ value. The drop in temperature as the flames at the surface disappear is clearly observed in the simulations. It is also visible in the experiments for $\dot{q}''_{ext}$ = 30 kW/m^2 and 50 kW/m^2, but it is hardly seen in the experiments for $\dot{q}''_{ext}$ =20 kW/m^2. After the dip, the temperature rises again, in good agreement with the experiments. The final decay phase has not really been measured in the experiments. In general, the trends are very well captured in the simulations.

Figure 2 shows similar results for wet MDF samples, containing 6.5% moisture [1], for $\dot{q}''_{ext}$ = 30 kW/m^2 and 50 kW/m^2. At the front surface, agreement between simulation results and experiments is very satisfactory. At depth d = 5 mm, the initial temperature rise, prior to pyrolysis, is well captured, as mentioned above. This indicates that, provided the moisture content of the sample is well-defined, the heat-up phase can be reproduced with a satisfactory level of accuracy. Agreement remains acceptable afterwards, although

the temperatures are over-predicted as long as the pyrolysis front has not reached d = 5 mm for $\dot{q}''_{ext}$ =30 kW/m^2. The over-prediction remains visible during pyrolysis for $\dot{q}''_{ext}$ = 50kW/m^2, but the trend is followed very well. The final decay phase seems too rapid at d = 5 mm, despite the very good agreement at the surface. This indicates that the material properties for char are not perfect in the sense that the thermal inertia is under-estimated.

Figure 3 shows the mass loss rate of the dry (left) and wet (right) samples. In all cases, the moment of onset of pyrolysis, indicated by the highest peak value, is very well predicted. This is due to the chosen pyrolysis temperature and the correct prediction of the thermal inertia during the heat-up phase. In all samples, the mass loss rate in the experiments, prior to the onset of pyrolysis, is related to evaporation of unbound moisture. This indicates that the samples, labelled as dry, are not truly completely dry. In the simulations, there is only mass loss rate prior to the onset of pyrolysis when moisture is explicitly taken into account. This then leads to a first peak in the simulations, related to the evaporation of the moisture. This first peak is too low, compared to the experimental values, e.g. 0.0043 kg/(m^2 s) at t = 8.5 s for $\dot{q}''_{ext}$ = 30 kW/m^2 in the simulations vs. 0.016 kg/(m^2 s) in the experiments. This does not strongly affect the results later on. In general, the experimentally measured mass loss rate is followed quite well in the simulations. The second peak, while predicted too early and being too wide, is predicted in the simulations, with the correct peak value in the mass loss rate. The global level of mass loss rate is also correctly predicted. This goes hand in hand with an accurate prediction of the duration of the pyrolysis process. In the simulations, the process stops suddenly, at the moment where the pyrolysis front reaches the back surface. In the experiments, this is a smoother transition. In the experiments, the total mass loss per unit

area ranges between 8.7 kg/m^2 and 9.5 kg/m^2 for the dry samples and between 9.4 kg/m^2 and 10.2 kg/m^2 for the wet samples. In the numerical simulations, the total mass loss per unit area equals the product of the material thickness and the difference between initial density and char density. This yields 9.1 kg/m^2 for the dry samples and 9.8 kg/m^2 for the wet samples.

The evolution of the mass loss rate strongly depends on the chosen value for pyrolysis heat, as is discussed next.

3.1.2 Sensitivity analysis

The sensitivity of the simulation results for mass loss rate to four model parameters is discussed now:

- heat of pyrolysis ΔQ_{pyr};
- surface emissivity ε;
- convection coefficient h;
- flame heat flux.

Dry samples are considered with an external heat equal to $\dot{q}''_{ext}$ = 30 kW/m^2. Only 1 parameter is changed at a time. The other parameter values are kept as described above.

Figure 4 (top left) shows the effect of heat of pyrolysis on the mass flow rate. The mass loss rate increases with decrease in the heat of pyrolysis, as the endothermic pyrolysis process consumes less energy, so that the pyrolysis front moves faster into the solid. An increase in mass loss rate results in a shorter pyrolysis stage. Clearly, the effect of ΔQ_{pyr} is substantial. The second peak even almost disappears when ΔQ_{pyr} is given a high value.

The effect of all other parameters is much smaller. Obviously a lower emissivity value leads to higher mass loss rates, as this factor is merely a loss term in the boundary

conditions (1). Note that we assume the imposed heat flux $\dot{q}''_{ext}$ as absorbed by the material constant here, which need not be true. If this were also considered, the effect of emissivity is smaller, and even in the opposite direction, as also less heat is absorbed, applying Kirchhoff's law.

The effect of the convection coefficient (bottom left picture) is only seen at the onset of pyrolysis. A higher value for *h* results in more heat loss at the front surface, so that the heat-up phase takes longer. As the material inside is then also already heated up more, the pyrolysis front moves faster during the early stages, leading to a higher first peak value in the mass loss rate. After a very short while in the pyrolysis process, the convection term becomes very small compared to all other terms, so that the effect of *h* becomes negligible.

The effect of the flame heat flux (bottom right picture) is visible, but not dominant. For obvious reasons, the mass loss rate increases and the pyrolysis stage becomes shorter as the flame heat flux increases.

3.2 Vertically upward flame spread

The set-up has been described in section 2.3. Figure 5 shows the visually observed evolution in time of the flame height, along with a possible parabola fit. The flame height was visually determined as the vertical position where there is a 'persistent flame'. It is important to note that during the early stages (t < 250 s and t < 60 s, respectively), the parabola is below the actually measured curve, while later it is above the curve. This is reflected in the results, as explained next.

Figure 6 shows the experimental and the numerical simulation results for the sand burner with constant heat release rate. At height y = 0 m, there is a simple evolution from the

initial temperature to the end temperature. The small variations at the onset of pyrolysis, after about 60 s, is due to the variation in the material properties, not due to a variation in boundary conditions (expressions (2a) and (2b)). Indeed, as $y < y_{pfr} = 0.4$ m, no heat flux is added due to the pyrolysis. Physically, this is due to a lack of oxygen to react with the released pyrolysis gases. All oxygen is already consumed by the methane fuel combustion by the sand burner. This also explains why the experimentally measured end temperature at $y = 0$ m is lower than e.g. at $y = 0.6$ m or $y = 1.2$ m. At $y = 0$ m, agreement between simulation results and experimental values is very good. Note that we did not try to model the extinguishing process by water mist in the experiments after 450s [1].

For the other heights, the prescribed time evolution of y_f is important. Indeed, we do not perform coupled pyrolysis – CFD simulations, but prescribe the evolution of y_f as obtained from the experiments. The sensitivity of the results to the accuracy of the representation of the time dependence of y_f is very clear. First examine the results at height y = 0.6 m. The flames reach this height during the early stages, so that the parabola fits lags behind the real curve. This is directly reflected in the results: the steeper temperature rise is too late with the parabola fit. With a piecewise linear reconstruction [1], agreement is not perfect, but much better. The evolution to the end temperature is well captured. This indicates that, provided the flame height and corresponding heat flux can be determined to a sufficient level of accuracy, e.g. by means of advanced CFD simulations, the pyrolysis model can be applied to simulate flame spread in the present configuration.

Similar findings are observed at $y = 1.2$ m. Five stages can clearly be distinguished:

- t < 120 s: heat-up phase due to the radiative incident heat from the sand burner;

- 120 s < t < 210 s: more rapid heat-up due to added radiative heat flux from flames; note that y_f < 1.2 m;
- 210 s < t < 290 s: still the same heat-up phase as mentioned above, but the material properties change as pyrolysis already starts in the simulations; note that still y_f < 1.2 m, as in the experiments no persistent flames were observed yet at this height;
- 290 s < t < 320 s: more rapid temperature rise because now y_f > 1.2 m;
- t > 320 s: pyrolysis is complete at y = 1.2 m and the temperature evolves towards the end value.

We consider the agreement between experiments and simulations results satisfactory, given the complexity of the set-up. Also for the other heights, the global trends are captured quite well in the numerical simulations.

Figure 7 shows essentially similar results, for the smaller inter-plate distance (10.5 cm) with the honey comb burner. Differences between the parabola fit and the real time evolution of y_f are smaller as everything evolves much faster.

4. Conclusions

Numerical simulation results, obtained by an enthalpy based pyrolysis model, were compared to experimental results of [1]:

- 1D cone calorimeter set-up for dry and wet MDF samples;
- 2D vertically upward flame spread for a parallel particle board plates set-up.

The simulation results are in general in good agreement with the experimental observations, provided the boundary conditions, material properties and model parameters are well-defined.

For the 1D set-up, a sensitivity study revealed the importance of the value for the heat of pyrolysis, while the influence of surface emissivity, convection heat transfer coefficient and flame heat flux is less pronounced.

For the vertically upward flame spread set-up for two parallel particle board plates, a physical explanation for the boundary conditions was given. In particular, the importance of re-radiation and the lack of oxygen to immediately combust the pyrolysis gases in between the plates were mentioned. Different stages, as observed in the simulations, were explained.

The importance of the accurate knowledge of flame height evolution in time was illustrated. The quality of the results indicates that, provided the flame height and corresponding heat flux are known, the present pyrolysis model can be used to simulate vertically upward flame spread in a parallel plate configuration.

5. Nomenclature

c	specific heat, $\left(J/(kg.K) \right)$
C	decay constant, (1/m)
F	correction factor,(-)
h	convection coefficient, $\left(W/(m^2 K) \right)$
k	conduction coefficient, $\left(W/(m.K) \right)$
L	*latent heat of vaporisation*, $\left(J/kg \right)$
$\dot{q}$"	*heat flux*, (W/m^2)
ΔQ_{pyr}	Heat of pyrolysis, $\left(J/kg \right)$
T	Temperature, $\left(\mathrm{K} \right)$

Subscripts

amb	ambient
c	char
ext	external
f	flame
pfr	persistent flame region
pyr	pyrolysis
surf	surface
v,w	virgin wet
v,d	virgin dry

Greek symbols

ρ	Density, $\left(kg/m^3\right)$
ε	Emissivity,(-)
σ	Stephan-Boltzmann constant, $\left(W/(m^2K^4)\right)$
τ	Time constant,(s)

6. Acknowledgements

This research is funded by project G.0130.06 of the Fund of Scientific research – Flanders (Belgium) (FWO-Vlaanderen). The experimental study was performed with financial support from from Lund LSF13 Project, Lund University, Faculty of Engineering, Combustion Physics, Lund, Sweden.

7. References

1. Wasan S. R., Van Hees P., Merci B., Study of Vertical Upward Flame Spread on Charring Materials – Part I: Experimental study, *Fire and Materials* (submitted).

2. Wasan S. R., Rauwoens P., Vierendeels J., Merci B., An enthalpy-based model for charring and non-charring materials in case of fire, *Combustion and Flame*, 2010, doi:10.1016/j.combustflame.2009.12.007.

3. de Ris J. L., Orloff L., Flame heat transfer between parallel panels, *Proc. 8th IAFSS Symposium*, pp. 999 – 1010 (2005).

4. Ingason H., de Ris J.L., Flame heat transfer in storage geometries, *Fire Safety Journal,* 1998; **31**: 39 – 60.

5. Wasan S. R., Rauwoens P., Vierendeels J., Merci B., Application of simple enthalpy-based model in numerical simulations of pyrolysis of charring materials, *Fire and Materials*, 2010; **34**: 39-54.

6. Lautenberger C., Fernandez-Pello C., A model for the oxidative pyrolysis of wood. *Combustion and Flame*, 2009; **156** (8): 1503-1513.

7. Delichatsios M., Paroz B., Bhargava A. Flammability properties for charring materials, *Fire Safety Journal*, **38** (2003), 219, 228.

8. Weng W. G., Fan W. C. A pyrolysis model of charring materials considering the effect of ambient oxygen concentration, *Fire and Materials*, 2007; **31**: 465-475.

9. SFPE Handbook of Fire Protection Engineering, 3rd Edition, 2002, *Chapter 1-4 Radiation Heat Transfer*.

Tables

$\rho_{v,w}$	$\rho_{v,d}$	ρ_c	$c_{v,w}$	c_v	c_c	h
735kg/m^3	690kg/m^3	140kg/m^3	2300J/(kg.K)	2000J/(kg.K)	2000J/(kg.K)	10W/(m^{2}K)
$k_{v,w}$	$k_{v,d}$	k_c	ΔQ_{pyr}	T_{amb}	T_{pyr}	ε
0.38W(m.K)	0.36W(m.K)	0.2W(m.K)	4 10^{5}J/kg	300K	598 K	0.9

Table 1. Model parameters and material properties for the cone calorimeter set-up for medium density fibre (MDF) board.

$\rho_{v,d}$	ρ_c	c_v	c_c	h	ε
600kg/m^3	60kg/m^3	2500J/(kg.K)	2500J/(kg.K)	15W/(m^{2}K)	0.9
$k_{v,d}$	k_c	ΔQ_{pyr}	T_{amb}	T_{pyr}	
0.36W(m.K)	0.23W(m.K)	8.7 10^{5}J/kg	300K	598 K	

Table 2. Model parameters and material properties for the parallel vertical plate set-up for particle board.

Distance	$\dot{q}''_{pfr}$	y_{pfr}	F	C_{pfr}	C_f	$\dot{q}''_f$
10.5 cm	30kW/m^2	0.8m	1/3	1.3m^{-1}	1.3m^{-1}	55kW/m^2
30.5 cm	37kW/m^2	0.4m	2/3	1.7m^{-1}	1.7m^{-1}	55kW/m^2

Table 3. Model parameters for inter-plate distance equal to 10.5 cm or 30.5cm.

Figures

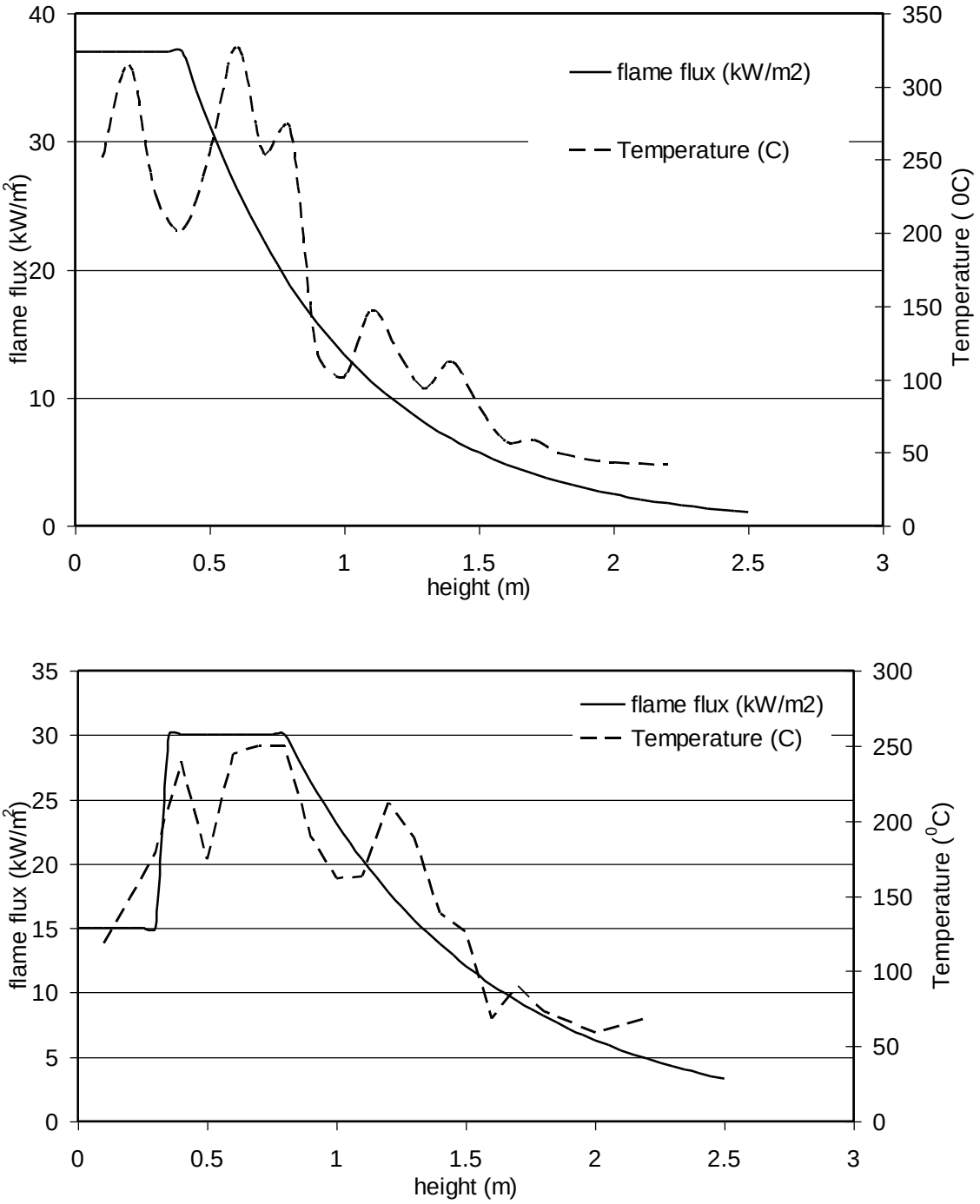

Figure 1. Imposed heat flux, prior to pyrolysis, for inter-plate distance equal to 30.5 cm (top) and 10.5 cm (bottom), along with temperature measurements.

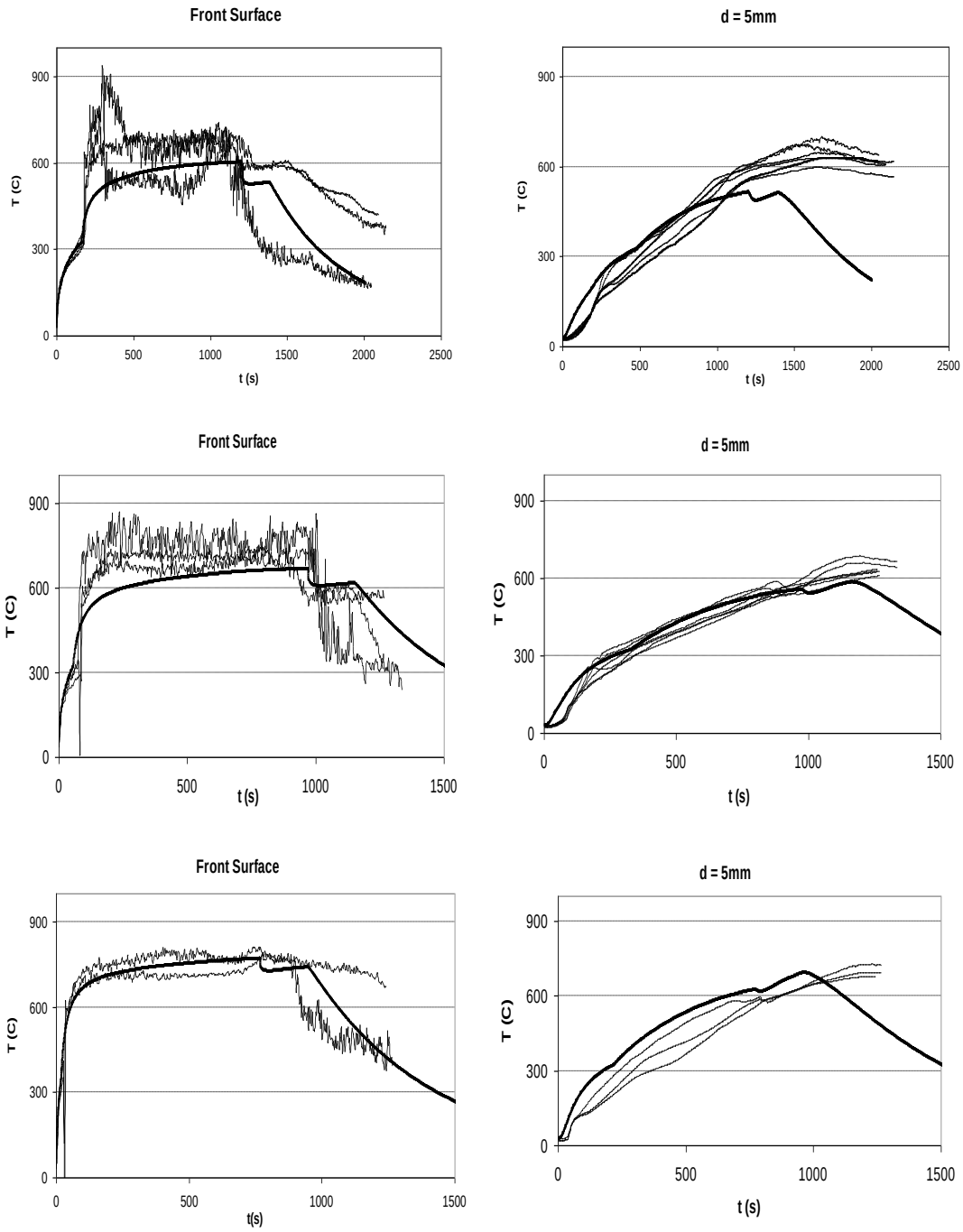

Figure 2. Evolution in time of temperature (dry sample). Left: front surface temperature; right: depth = 5mm. Top: $\dot{q}''_{ext}$ = 20kW/m^2; middle: 30kW/m^2; bottom: 50kW/m^2. Thick line: numerical simulations; thin lines: experiments.

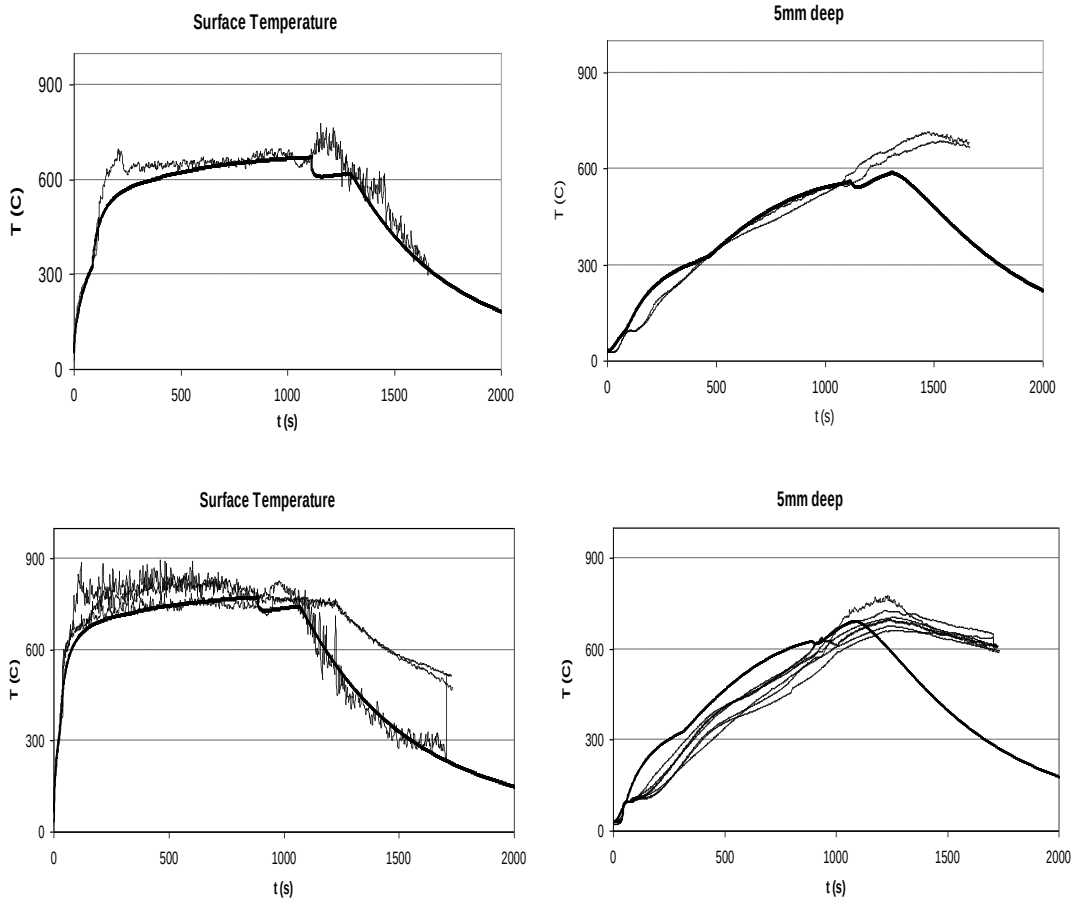

Figure 3. Evolution in time of temperature (wet sample). Left: front surface temperature; right: depth = 5mm; bottom left: depth = 8mm. Top: $\dot{q}''_{ext}$ = 30kW/m^2; bottom: 50kW/m^2. Thick line: numerical simulations; thin lines: experiments.

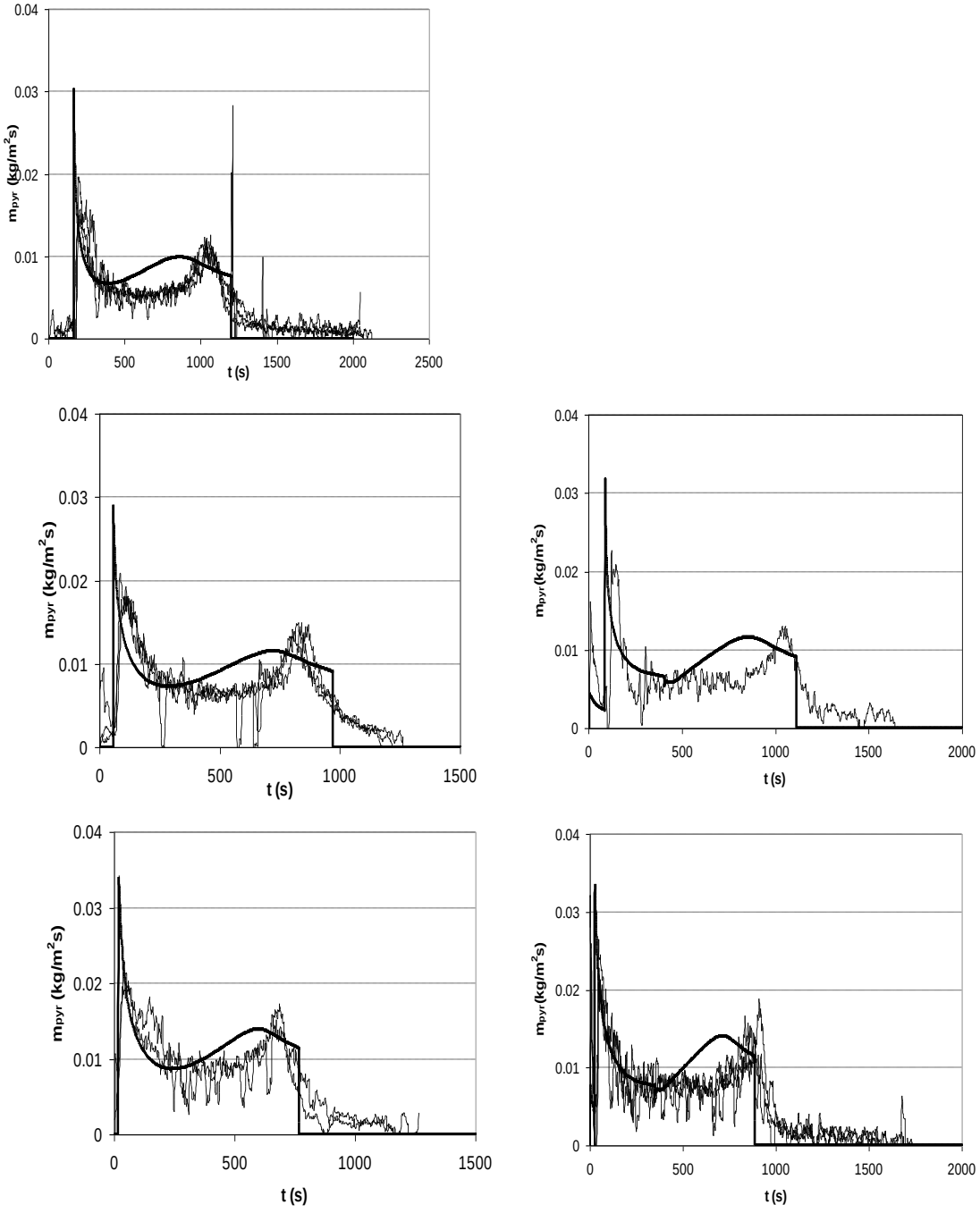

Figure 4. Evolution in time gas mass flow rate for dry samples (left) and wet samples (right). Top: $\dot{q}''_{ext}$ = 20kW/m^2; middle: 30kW/m^2; bottom: 50kW/m^2. Thick line: numerical simulations; thin lines: experiments.

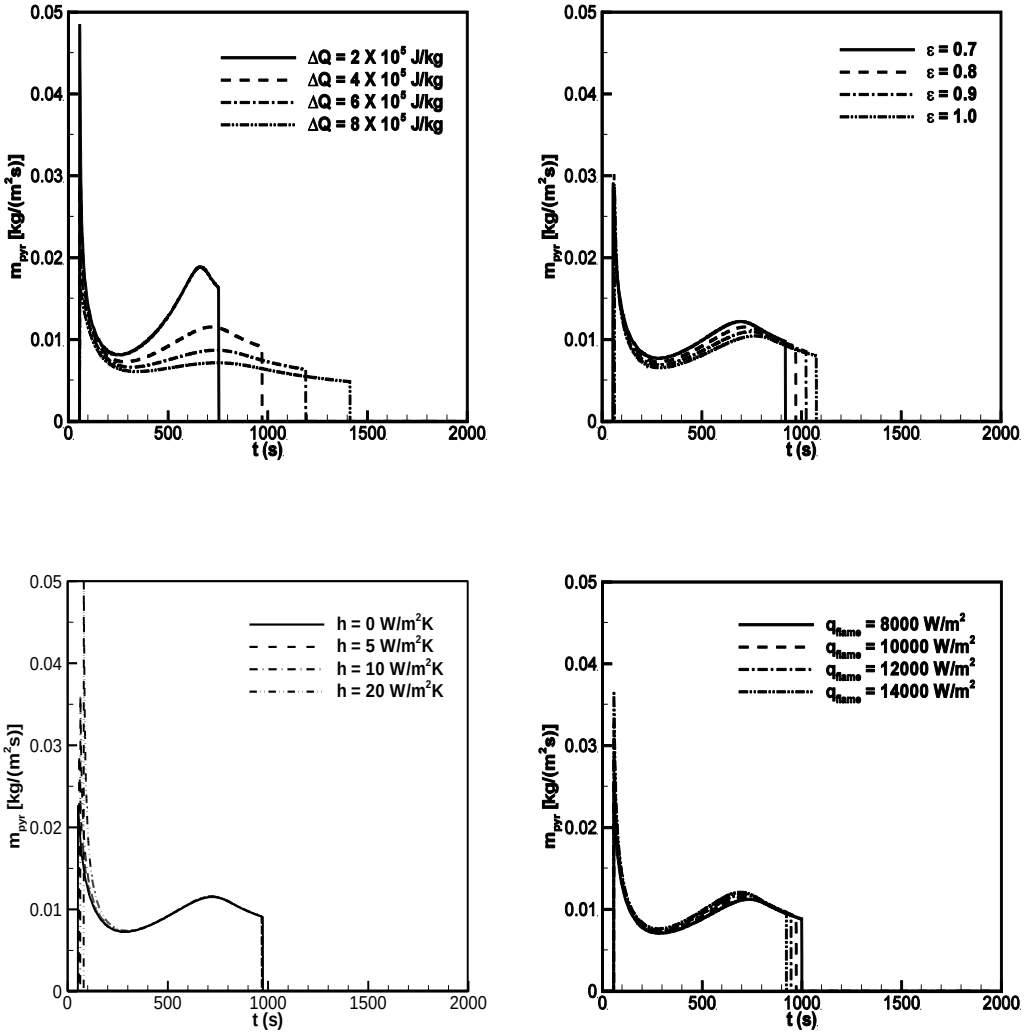

Figure 5. Sensitivity of mass loss rate evolution to model parameters (dry samples, $\dot{q}''_{ext}$ =30kW/m^2). Top left: Heat of pyrolysis; top right: surface emissivity; bottom left: convection coefficient; bottom right: flame heat flux.

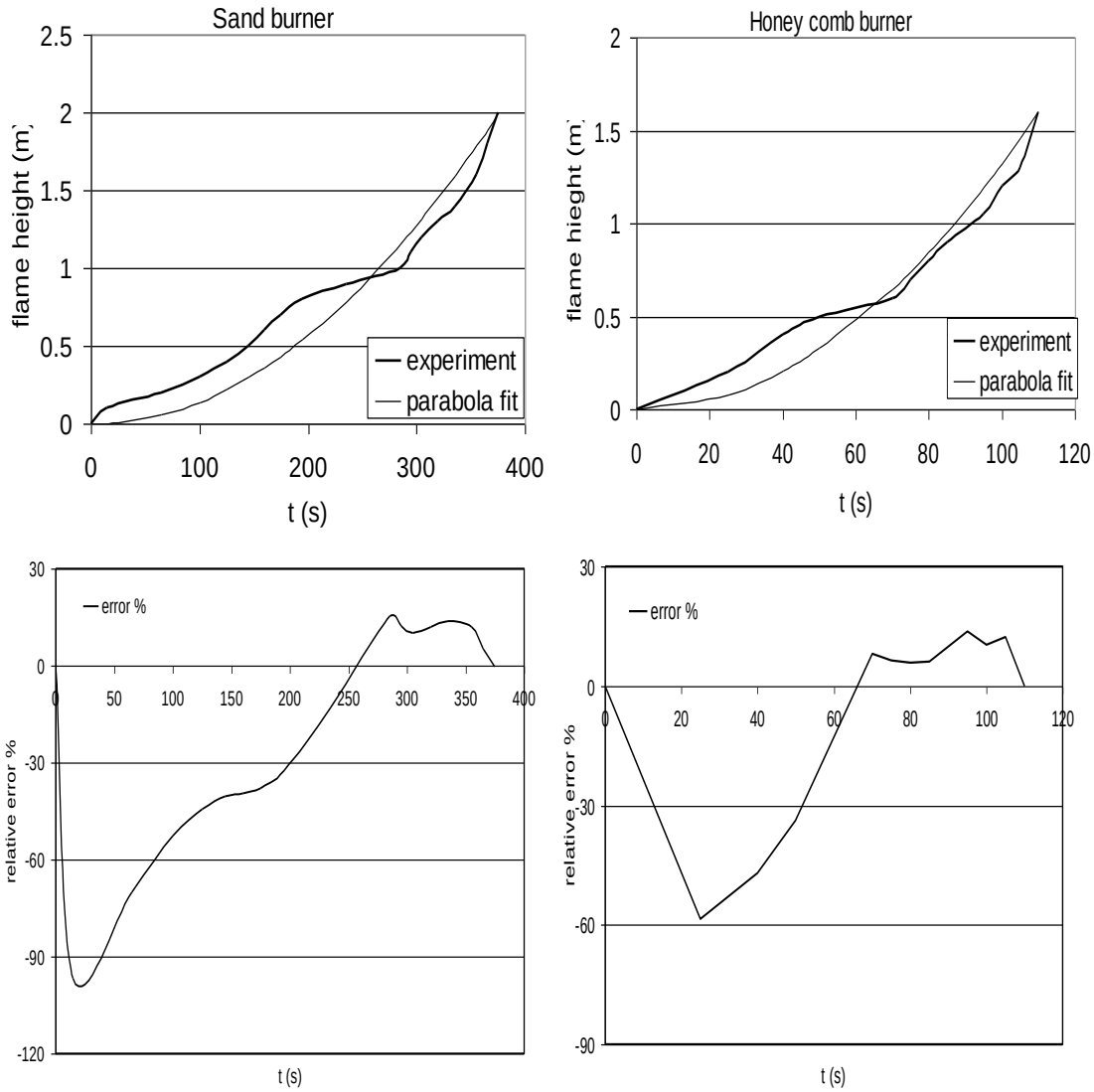

Figure 5. Flame height evolution in time (top) and relative error of parabolic fit, compared to the experimental value (bottom). Inter-plate distance equal to 30.5 cm (left) and 10.5 cm (right).

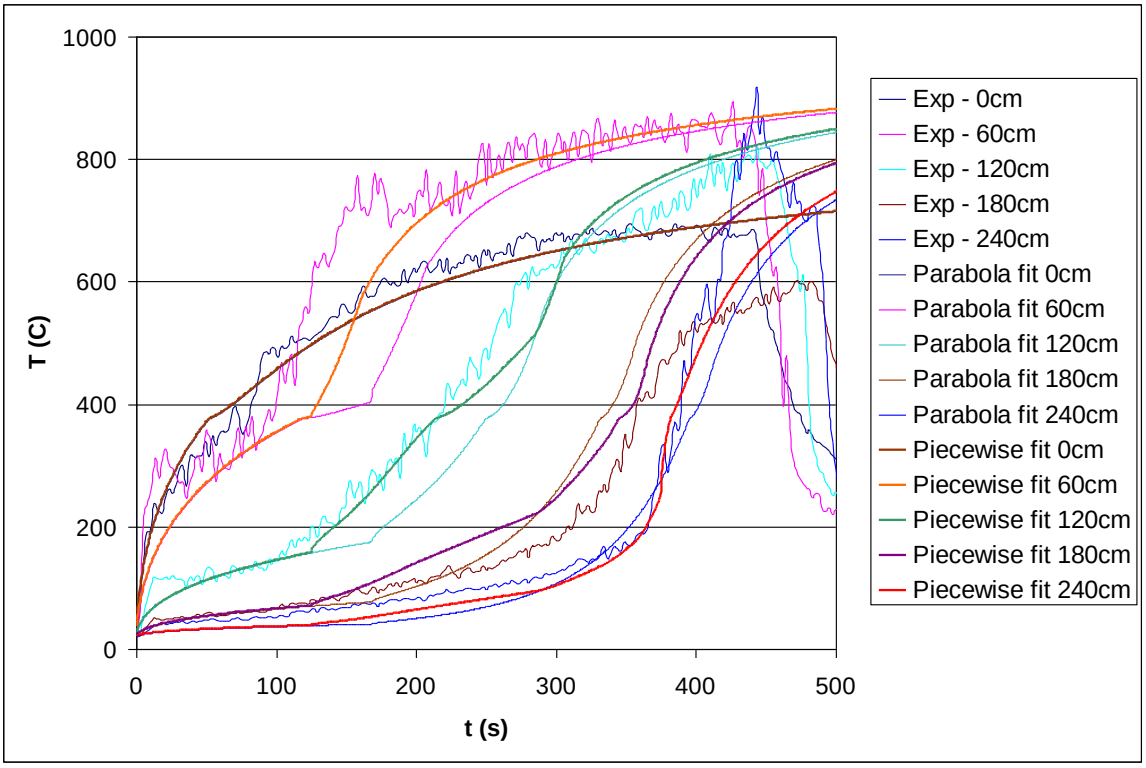

Figure 6. Temperature evolution for different heights (inter-plate distance 30.5 cm).

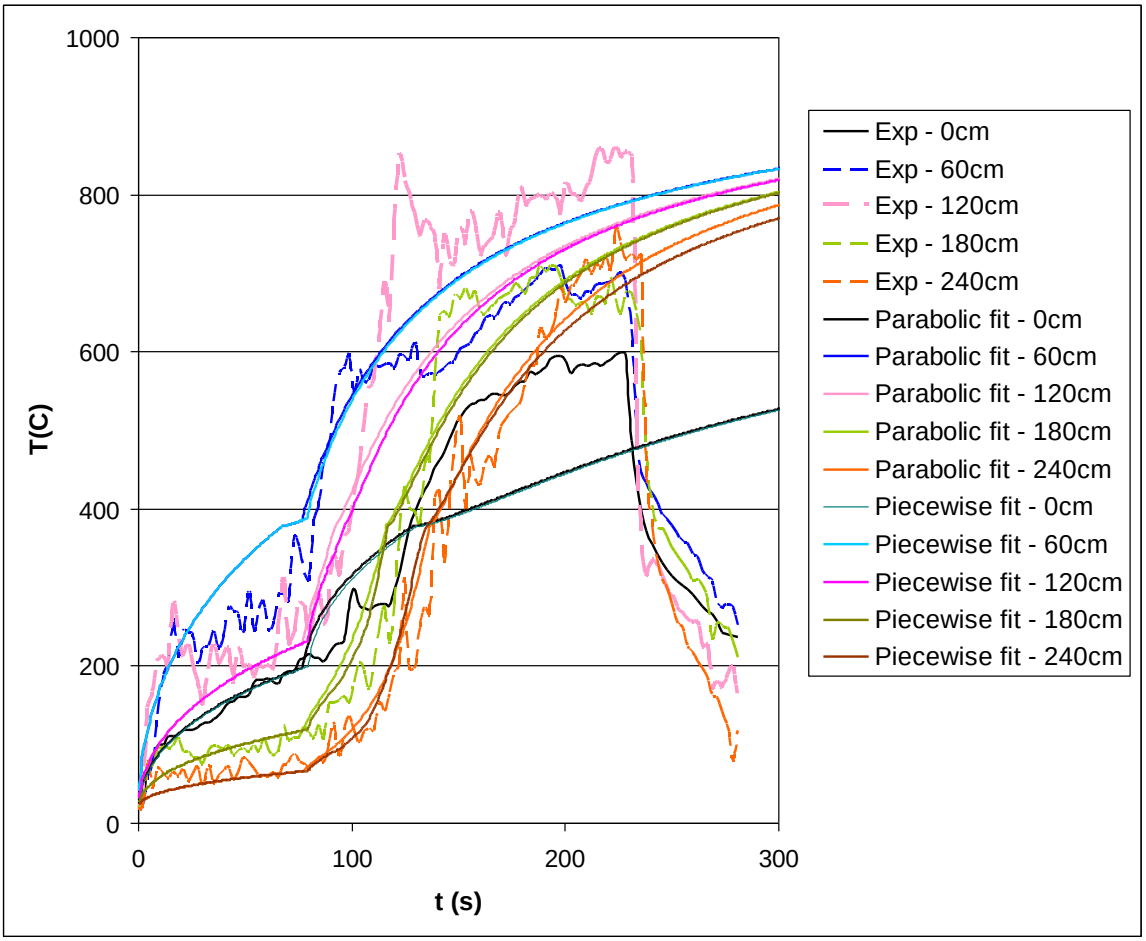

Figure 7. Temperature evolution for different heights (inter-plate distance 10.5 cm).